Materials & Design 213 (2022) 110330

Contents lists available at ScienceDirect

Materials & Design

journal homepage: www.elsevier.com/locate/matdes

Electrical resistance flash sintering of tungsten carbide

Isacco Mazo [a,*], Alberto Molinari [a], Vincenzo M. Sglavo [a,b]

[a] University of Trento, Department of Industrial Engineering, Via Sommariv 9, 38123 Trento, Italy
[b] INSTM, Trento Research Unit, Via G. Giusti 9, 50123 Firenze, Italy

HIGHLIGHTS

- The interaction of an electric current with the electrical properties of tungsten carbide green bodies triggers the conditions for flash sintering, which results in ultrafast densification up to 95% in less than 10 s.
- A thermal runaway of Joule heating is activated by the negative temperature dependence of resistivity of the material in the green state.
- Flash sintering of tungsten carbide is characterized by the absence of an incubation stage and by a self-extinguishing power surge.
- The microstructure achieved after the flash can be tailored and optimized by prolonging the sintering into a resistive heating regime, thus increasing the final density further, as well.

GRAPHICAL ABSTRACT

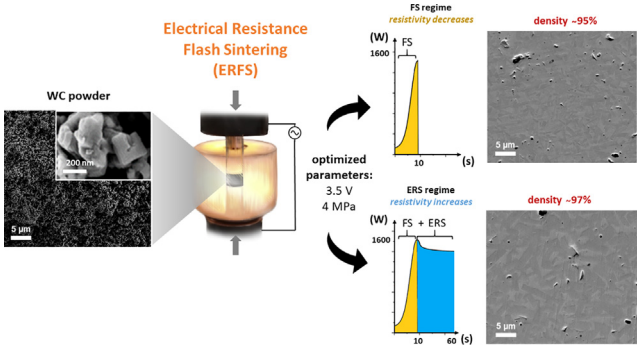

ARTICLE INFO

Article history:
Received 24 September 2021
Revised 16 December 2021
Accepted 16 December 2021
Available online 18 December 2021

Keywords:
Binderless tungsten carbide
Pressure assisted flash sintering
Electrical resistance sintering
Electrical properties
Positive temperature coefficient for resistivity

ABSTRACT

This work explores the possibilities for the ultrafast sintering of binderless tungsten carbide by electric/-pressure assisted sintering. A limited voltage (3–4 V) in AC condition was applied to WC powder compact in combination with uniaxial pressure. The thermal insulating ceramic die allows the ultrafast heating (10^4 °C/min) of the powder compact which undergoes a rapid transition of its electrical properties, from negative to positive dependence of resistivity on temperature, i.e. from NTC to PTC behaviour. Such effect is fundamental for inducing a thermal runaway phenomenon associated with ultrarapid temperature increase and massive electric power dissipation, thus inducing very rapid sintering. The relationship between electrical properties of tungsten carbide and the possibility to achieve "flash sintering" conditions to complete densification in a couple of seconds was investigated. At the optimal conditions of 3.5 V and 4 MPa pressure, pure WC sinters up to 95% in less than 10 s. Longer sintering time after the flash improves only slightly the density, despite a significant energetic consumption. It is also shown that if larger pressure is applied, the flash event duration and final density decrease.

* Corresponding author.
E-mail addresses: isacco.mazo@unitn.it (I. Mazo), alberto.molinari@unitn.it (A. Molinari), vincenzo.sglavo@unitn.it (V.M. Sglavo).

https://doi.org/10.1016/j.matdes.2021.110330
0264-1275/

1. Introduction

Tungsten carbide (WC) is a relevant material in the manufacturing of steels and metal alloys due to its outstanding hardness and stiffness. In the last 60 years, the research has been focused on the possibility to enhance WC intrinsic brittleness and poor sinterability by the activation of liquid phase sintering through the incorporation of limited amount of Co or Ni [1,2]. The poor oxidation resistance and the loss of hardness at high temperature of the metallic phase has lead the researchers to the development of metal-free or binderless tungsten carbide (BTC) [3,4]. The strong covalent chemical bonds and the low diffusion of carbon atoms represent fundamental issues in WC processing. Traditional pressureless sintering is unsuccessful, it requiring temperature above 2000 °C and long times which account for coarse microstructures [5]. Even hot isostatic pressing (HIP) and hot pressing (HP) require grain growth inhibitors to control the sintering kinetic and limit coarsening [6–8]. Recently, binderless production has been enhanced by innovative techniques like spark plasma sintering (SPS) where the application of a high current density combined with uniaxial pressure allows the complete densification of the starting pure WC powder in 10–30 min. In this way, it is possible to obtain monophasic (hexagonal), dense (≥98–99%), stiff (≈700 GPa), and hard (26–30 GPa) materials without the use of any sintering aids [9–11]. In spite of said outstanding properties, the possible uses of binderless WC are restricted to applications not exposing the material to violent and unexpected loads, like wear components, drawing dies, corrosion resistant mechanical seals, friction parts, optical glass moulds and high temperature electrical contacts. In addition to said limitations, the use of the graphite die as heating element in SPS strongly limits productivity and freedom in component geometry. BTC intrinsic brittleness makes its use in the manufacturing industry impossible as a possible substitute of the cemented carbide counterpart (WC-Co/Ni)[12]; as a matter of fact, the typical fracture toughness of BTC produced by SPS is in the range of 4–6 $MPam^{0.5}$ while cemented counterpart can achieve values three times larger, 10–16 $MPam^{0.5}$ [13]. As recently pointed out by Sun et al., [4] the rapid production of fully dense and high toughness sintered bodies is the biggest challenge for the development of BTC.

In this perspective, the consolidation of ceramics under "flash sintering" conditions has revealed an enormous potentiality since (i) it allows the complete densification of ceramics in few seconds with an enormous saving in the required energy [14,15] and (ii) it allows to process materials with new and/or improved functional and structural properties [16,17]. Several studies indicate how flash sintered ceramics possess peculiar microstructures, out of equilibrium phases and even enhanced plasticity accounted for by defects chemistry modification [18–21]. The flash sintering phenomenon occurs at an onset combination of electric field and furnace temperature, forcing an electrical current through the material, responsible for a thermal runaway of Joule heating. The thermal runaway is a non linear event characterized by extremely high heating rates [22,23] which has been successfully modelled by Zhang et al. [24] and Todd et al. [25] in electronic (ZnO) and ionic conductors (3YSZ), respectively. The enormous heating rates of about 10^4 °C/min developed during such event was found to be responsible for a large boost in the sintering rate [26–28].

According to the existing theories, the flash event cannot occur in materials characterized by a positive temperature coefficient (PTC) for resistivity like metals or, for example, tungsten carbide (WC). In spite of that, Grasso et al. [29] and McKinnon et al. [30] found evidence of ultrafast sintering of PTC ceramics, like ZrB_2 and TiB_2/hBN. McWilliams et al. [31,32] recently discovered the activation of a flash event in a metallic Al powder due to the presence of a surface oxide layer and the rapid transition of the compact from insulator to conductor. Heating rates in the order of 10^3-10^4 °C/min, as found during the flash event in Al powder, was proposed to excite certain phonons more than others, thus allowing the generation of point defects far beyond the equilibrium concentration. Jongmanns and Raj [33] simulated how driving an Al single crystal lattice out of equilibrium by nonlinear lattice vibration can lead to this proliferation of interstitials and vacancies which promotes ultrafast sintering.

The possibility to activate a flash event in aluminium powder and the ultrafast sintering of PTC ceramics similar to WC, stimulated the following question: is it possible to trigger a *flash like event* also in pure tungsten carbide?

The present work aims to explore the interaction of an alternated current with WC green bodies and the conditions, if existing, to activate ultrafast sintering. More in detail, the conditions for (i) non linear variation of the electrical resistivity, (ii) abrupt increase of the electrical power dissipation, (iii) heating rate as high as 10^4 °C/min and (iv) sintering rates which can allow densification in few seconds are investigated. In order to achieved these results, pure tungsten carbide was tested in a specifically designed pressure assisted-flash sintering apparatus [34,35]. To fully prove the occurrence of a flash event, sintering experiments were carried out taking care of (1) not changing the native electrical properties of the powder, (2) promoting exclusive interaction of the electrical current with the material to be tested, (3) accurate in situ monitoring of the phenomenon and (4) large current density capabilities of the contacts electrodes. Therefore,

1. the starting WC powder was not treated, green samples for sintering tests were uniaxially pressed without addictives and without a presintering;
2. the graphite die used in SPS was substituted with an insulating ceramic die;
3. a fast data acquisition system was developed for monitoring sintering shrinkage, temperature, resistivity and electrical power dissipation;
4. flash sintering experiment was performed on pellets [15], where the flat punches for applying pressure serve also as electrodes.

In this way, differently with respect to SPS, possible superimposed electro-thermal effects between the material and the graphitic die are eliminated [36]. In addition, important information on flash sintering behaviour of conductive material like tungsten carbide can be obtained.

2. Experimental procedure

Commercially available nanocrystalline WC powder (Inframat Advanced Materials) with an average particle size of 150–240 nm (Fig. 1(a)) was used in the present work. According to preliminary XRD analysis (Fig. 1(b)), the powder is mainly composed of α-WC (crystallite size ~ 40–70 nm) with limited amount of tungsten oxides (WO_3 and WO_4H_2). The powder was uniaxially pressed (350 MPa) in a steel mould by a manual hydraulic press (Specac) to produce cylindrical pellets with 6 mm diameter and thickness between 3 and 8 mm. The different thickness was obtained just by using different amount of powder. The average relative density of the green specimens was 40%.

The apparatus used for the sintering experiments is shown in Fig. 2. It consists of a modified mechanical testing machine (MTS System, model 810) whose load cell and lower piston are connected to two copper/molybdenum electrodes. The green sample (WC pellet) is inserted into an insulating die made of partially sta-

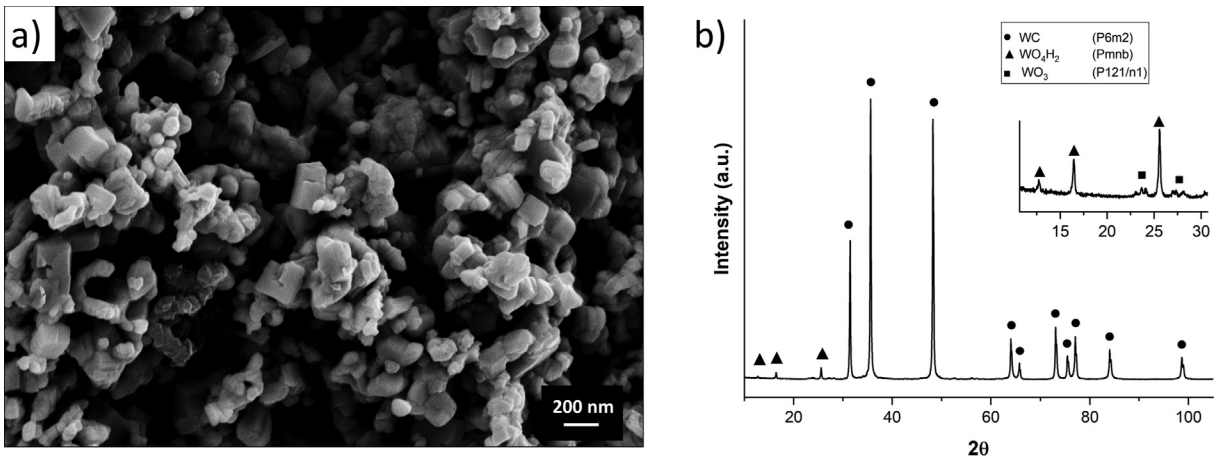

Fig. 1. SEM micrograph (a) and XRD spectrum (b) of the tungsten carbide powder used in the present work.

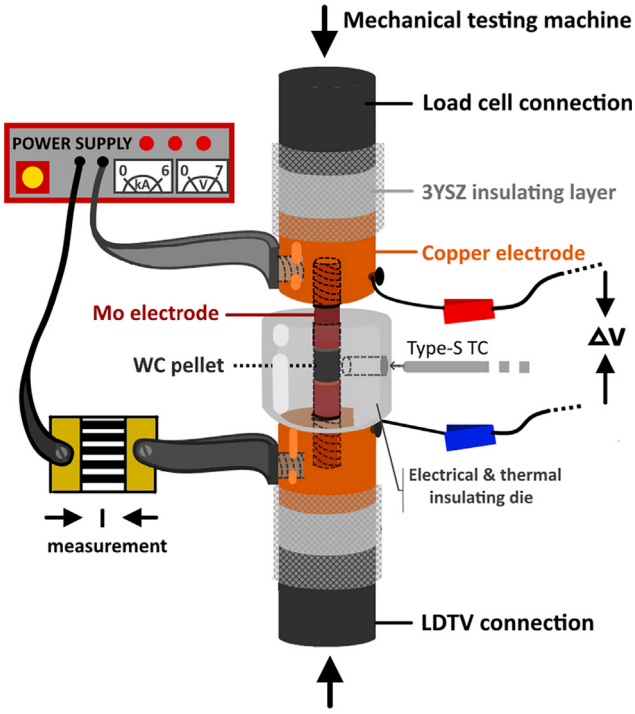

Fig. 2. Apparatus used for the sintering experiments.

bilized zirconia (3YSZ) and pressed by the electrodes; the ceramic die forces the electrical current to flow only through the specimen and avoids rapid heat loss generated during the experiment [37].

The mechanical testing machine is equipped with a load cell and a linear differential transducer (LVDT) to record the applied load and the vertical displacement, which enables to evaluate the pressure applied to the pellet and the shrinkage during sintering. An AC, 50 Hz, power supply (TECNA item 3870) is connected to the electrodes to provide the electrical power. Sintering experiments were performed under an electric field ranging between 3 and 9 V/cm for 10 and 60 s and a current density between 2.8 and 4.5 kA/cm^2. Two different contact pressures (4 and 60 MPa) and three different voltages (3, 3.5 and 4 V) were used. Each combination was run in triplicate to assess the repeatability of the experiment.

After being extracted from the 3YSZ die, the sintered WC samples were sectioned axially by a diamond blade, mounted in resin and polished progressively with diamond abrasives down to 1 μm. The microstructure was analyzed by a digital optical microscope (Olympus OLS5000) and by SEM (JEOL IT300) on fresh fracture surface and polished cross sections. Density and apparent porosity were measured according to the Archimedes' method (ASTM C373-17) using a precision balance (Kern ALJ 310 4A).

The evolution of the electrical parameters during sintering was measured directly on the WC sample, according to the electrical configuration shown in Fig. 3(a). A multichannel data acquisition system (DAQ NI USB 6211) scanned almost simultaneously voltage and current. The voltage difference was acquired between the two copper electrodes, as shown in Fig. 2. The current was measured by placing a calibrated shunt resistance (2500 A, 60 mV) in series with the circuit. The acquisition was carried out by LabView software, sampling the two alternated signals at 100 ksample/s. Voltage and current root mean square (RMS) values were evaluated with an average integration cycle of 0.02 s. The temperature was measured by placing a type S thermocouple in contact with the pellet, laterally within the zirconia die through a 4 mm hole produced halfway up its height (Fig. 2). A digital multimeter (Keithley DMM6500) equipped with an acquisition card for thermocouples (2001 TCSCAN CARD) performed the temperature recording at around 50 readings/s.

The influence of pressure on the resistivity of green pellets was measured within the zirconia die by using the electrical configuration shown in Fig. 3(b). The resistance was measured in a 4 point configuration while increasing the pressure from 0 to 100 MPa, with a high resolution (1 μΩ) multimeter (Keithley DMM6500). The resistive contribution of the electrodes in contact with the specimen was subtracted from the resistivity data [38].

The effect of temperature on the resistivity of both WC green pellets and bulk material was analysed within a dilatometer (Linseis DIL L75 PT), heating the material from 25 to 1550 °C (10 °C/min) under argon atmosphere. In this case, the green specimen was inserted in an alumina tube (Fig. 4 (a)) and four shielded platinum wires were placed in contact with it to generate a 4 point configuration. The shrinkage of the pellet was also measured upon heating. The bulk resistivity was measured as a function of temperature using the configuration shown in Fig. 4(b). Fully dense (99%+) 20 mm diameter disks were produced by SPS (Dr. Sinter 1050) at 2100 °C with 5 min holding time and 200 °C/min heating rate. Small bars (13x4x1 mm^3) were machined from such disks, placed in a small tubular furnace and connected by four shielded platinum wires to the multimeter.

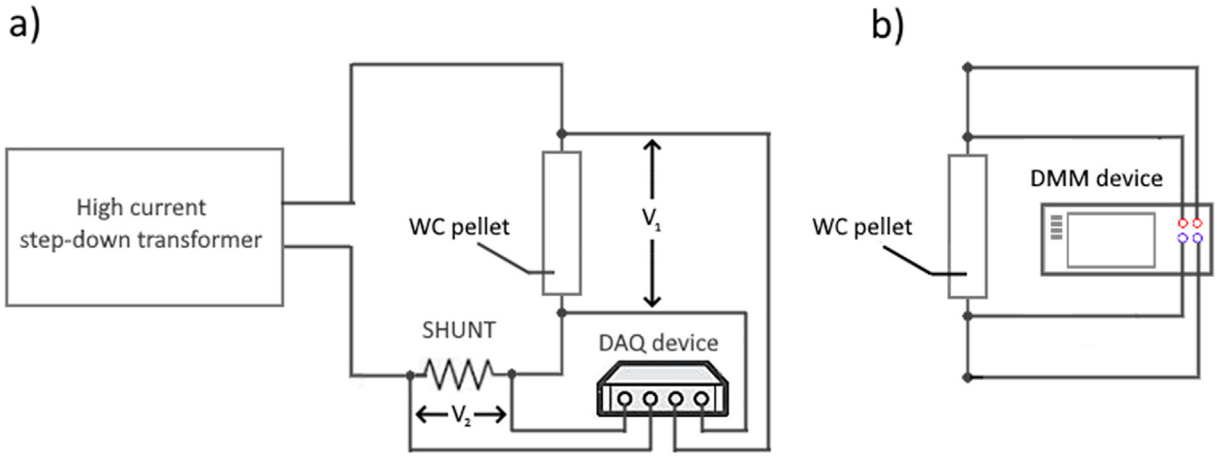

Fig. 3. Configurations used for the acquisition of electrical data on pellet sample within the die: voltage and current measurement during sintering experiments (a); 4-point resistance measurements at different pressures (b). (TC = thermocouple).

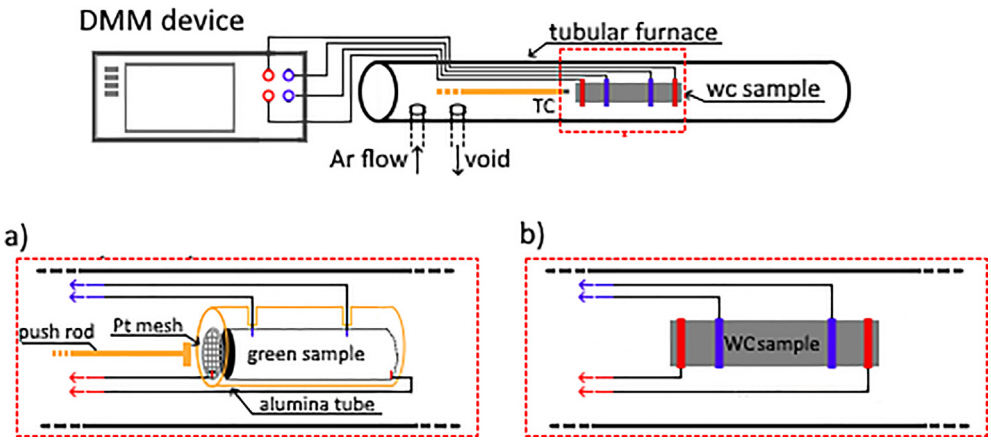

Fig. 4. Apparatus used to measure the electrical resistivity as a function of temperature of the green sample (a) and the bulk specimen (b).

3. Results & discussion

3.1. Flash event in pure tungsten carbide nanopowder compact

The application of an alternated current to the tungsten carbide green sample induces a rapid evolution of the electrical and physical properties. As shown in Fig. 5, the applied voltage decreases from about 3 V to 1 V while the current increases from 40 A up to 800 A in less than 10 s. This behaviour corresponds to a very rapid change in the material resistivity, which decreases by three orders of magnitude from $6.7x10^{-3}\Omega m$ to $7.6x10^{-6}\Omega m$ in the same time interval; then, it remains almost constant until the end of the sintering experiment. Correspondingly, the absorbed electrical power reaches a maximum of about 1000 W (9800 mW/mm^3) and it slightly decreases to 850 W afterwards. As clearly reported in Fig. 5(c), the observed sudden variation of the material resistivity is also associated with (i) a very rapid increase of its temperature, which reaches values in excess of 1720 °C, as proven by the thermocouple tip melting, and, more importantly, (ii) an abrupt shrinkage of the sample (about 20%) in the first 10–12 s. The estimated heating rate is exceptionally high with an average of 20,000 °C/min in the first 9 s and a maximum value of about 50,000 °C/min. The real phenomenon occurring during this rapid evolution of the power dissipated is shown in Video 1, where the exponential temperature increase of the pellet is directly observable from the zirconia die. Just as a reference, similar heating rates (in the order of 10^4°C/min) have been estimated during the thermal runaway of flash sintered ceramics [14,15,23,26,39–41]. Based on the features pointed out so far, the observed phenomenon can be defined as Electrical Resistance Flash Sintering (ERFS).

Fig. 6 (a) shows the evolution of the WC pellet during the electrical current assisted sintering test. After 60 s, the density evolves from 40% up to 75% under 1000 W maximum power peak and 4 MPa pressure. Both thickness and diameter of the specimen sensibly decrease, the latter becoming smaller in the central region. Such anisotropic effect can be accounted for by the very different thermal conductivity of molybdenum (138 W/m K) with respect to zirconia (1–3 W/m K) which induces a larger dissipation of the internally generated heat through the electrodes, thus making sintering less efficient on the top and bottom portions of the pellet. Correspondingly, the sintered component appears denser in the mid height region, as revealed by the observation of pellet cross section (Fig. 6(b)), which points out the presence of some residual porosity.

The sintering rate $\dot{\varepsilon}$ during the ERSF process can be determined as:

$$\dot{\varepsilon} = \frac{1}{\rho}\frac{d\rho}{dt} \tag{1}$$

where ρ is the density. Since the electrodes act as constraints for sintering on the top and bottom region of the pellet, the evaluation of the sintering rate has to take said non isotropic shrinkage

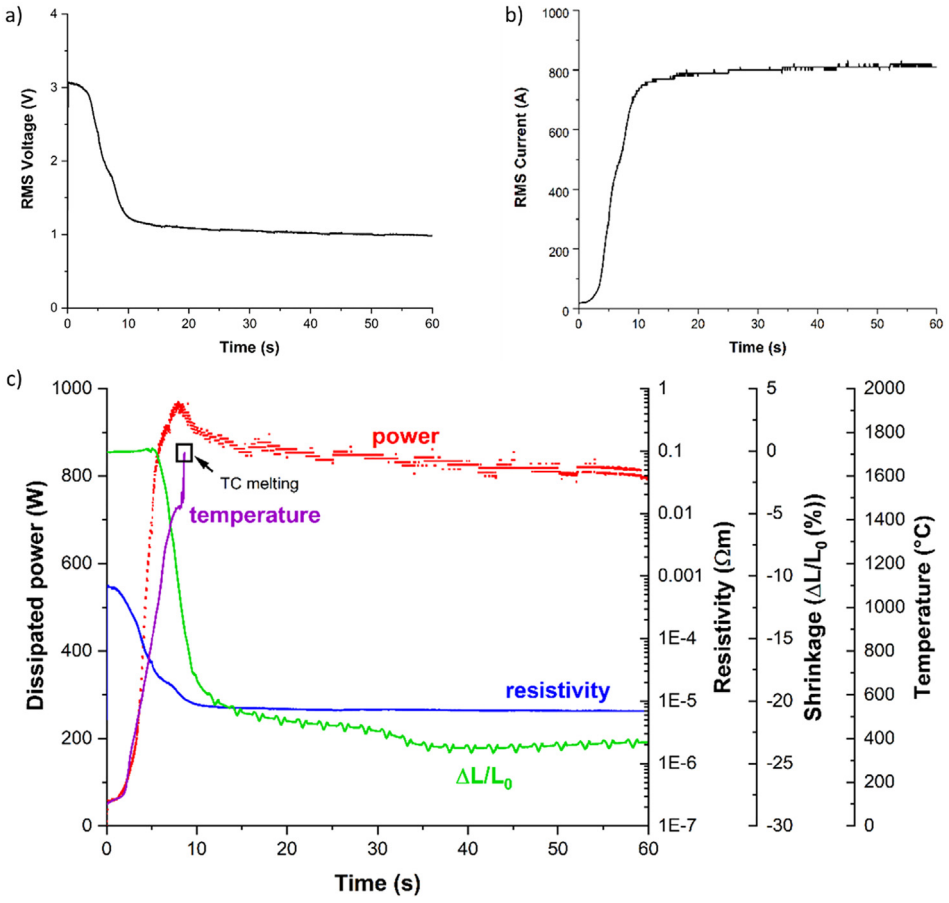

Fig. 5. Data acquisition during the test of a WC pellet under 3 V and 4 MPa; a) voltage, b) current, c) dissipated power, resistivity, shrinkage and temperature.

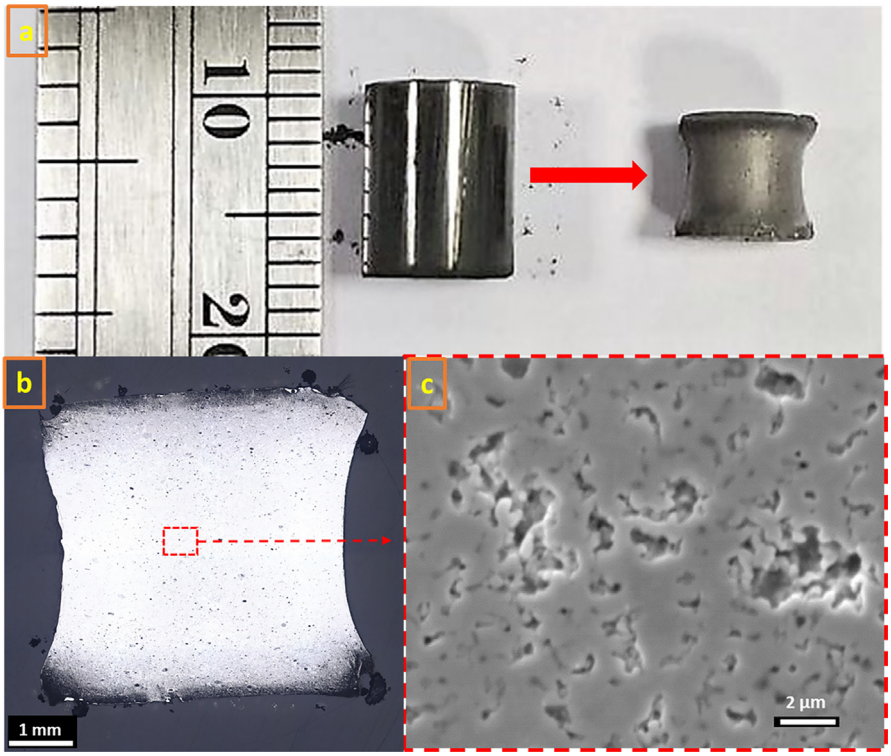

Fig. 6. WC sample before and after the sintering experiment (3 V, 4 MPa, 60 s) (a); optical (b) and SEM (c) micrographs of polished cross section after sintering.

into account. For this reason, two limiting cases can be considered for the evaluation of density and sintering rate corresponding to (i) the pellet maintaining the original diameter (with axial shrinkage, only) and (ii) isotropic shrinkage.

In the former case, the density can be calculated as:

$$\rho = \frac{\rho_0}{\varepsilon + 1} \tag{2}$$

where ε is the shrinkage and ρ_0 the green density. In the case of isotropic shrinkage, the density is instead:

$$\rho = \frac{\rho_0}{(\varepsilon + 1)^3} \tag{3}$$

If the shrinkage is equal to the axial one ($\Delta L/L_0$) as reported in Fig. 5, the sintering rate can be estimated by Eqs (2) and (3) and plotted as in Fig. 7, together with the dissipated electrical power. It is possible to observe that the maximum sintering rate is achieved exactly at the power peak. At this point, since the real shrinkage of the pellet is non isotropic, the real sintering rate must fall between the two limiting rates just pointed out. In any case, an exceptionally high sintering rate between 400 and $1200x10^{-4}s^{-1}$ can be determined during the power surge, this being one to three orders of magnitude larger with respect to traditional and even spark plasma sintering processes carried out on pure tungsten carbide [26,42].

Ultra fast firing, where heating rates approach 10^4 °C/min, like in the present situation, has been demonstrated to increase sintering rates by two or more orders of magnitude [26,43,44]. The extremely rapid temperature upsurge, in concomitance with the electrical power peak generated by a non linear drop in the material resistivity, suggests the occurrence of an electrical runaway of Joule heating phenomenon like in flash sintering of ceramics [15,23,39,45–48]. Nevertheless, a profound difference has to be pointed out between typical flash sintering of ceramics and the phenomenon of interest here because the former has been identified on materials characterized by negative temperature coefficient (NTC) for resistivity while tungsten carbide shows an opposite behaviour.

3.2. Conditions for the flash sintering in a PTC ceramic

Fig. 8(a) shows the evolution of resistivity as a function of temperature for bulk tungsten carbide, the data at low temperature having been collected from the literature [49]. A clear PTC behaviour is shown, the resistivity increasing from $2.2x10^{-7}$ to $1.5x10^{-6}\Omega m$ from room temperature up to 1550 °C. Differently from typical metallic materials, the resistivity of bulk WC follows an Arrhenius like temperature trend according to the relationship (Fig. 8(b)):

$$\rho = \rho_0 e^{\frac{Q}{RT}} \tag{4}$$

where Q is the activation energy for conduction, equal to $-6151(J/mol)$ and $\rho_0 = 2.13x10^{-6}\Omega m$ the pre-exponential factor.

At this point, the energetic model proposed by Todd et al. [45] and Zhang et al. [24] to describe the thermal balance between the heat generated by Joule heating, "W_{in}" (current flow through the material), and the heat dissipated by radiation, "W_{out}", through the specimen surface as a function of the "furnace, T_0" and "sample,T " temperature can be considered:

$$W_{in} = \frac{E^2 \pi r_0^2}{\rho_0} e^{\left(-\frac{Q}{R(T_0+\Delta T)}\right)} \tag{5}$$

$$W_{out} = 2\pi r_0 \sigma \varepsilon ((T_0 + \Delta T)^4 - {T_0}^4) \tag{6}$$

where the "sample" temperature is expressed as $T = T_0 + \Delta T$, r_0 is the radius of a cylindrical specimen, σ the Boltzmann constant and ε the emissivity.

As shown qualitatively in Fig. 9(a), the PTC for resistivity identified for WC is always responsible for an equilibrium condition between the two said power forms which allows the sample to reach a specific and finite temperature value that strongly depends on the applied voltage or current. This is substantially different with respect to the behaviour shown by materials characterized by NTC for resistivity. In this case, as shown in Fig. 9(b), a critical condition can be reached at a specific combination of electric field (E) and furnace temperature, corresponding to the thermal runaway for Joule heating, which determines an abrupt increase in the "sample" temperature and accounts for very rapid sintering of the material.

According to the considerations previously reported, it is possible to point out that in the present work the resistivity evolution with temperature is the key to activate a thermal runaway phenomenon [14,15,45,48,50].

Fig. 10 shows how the resistivity of the green WC pellet changes with temperature during heating, the diagram indicating a clear NTC behaviour, differently from the behaviour previously observed for the bulk material (Fig. 8). The electrical resistivity decreases from $10^{-3}\Omega m$ down to $10^{-5}\Omega m$ as the temperature increases from about 100 °C to 900 °C. The largest resistivity drop is recorded below 900 °C, well before densification (1050 °C) occurs: more in detail, an initial decrease is observed between 200 and 800 °C followed by a steeper reduction between 800 and 900 °C. When the sample starts to shrink, resistivity drops further this being accounted for by a porosity diminution corresponding to a density increase of about 7%. Upon cooling, the resistivity is affected only by a temperature dependence, reaching a final value of $1.8x10^{-6}\Omega m$. It is interesting to observe the relatively small difference between the resistivity of 40% dense material (as it was obtained after the thermal cycle in Fig. 10) and fully dense WC, i.e. from $10^{-6}\Omega m$ to $10^{-7}\Omega m$.

The results pointed out according to Fig. 10 can lead to the following conclusions: i) a significant drop in resistivity occurs in WC nanoparticles green compact upon heating and ii) the effect of porosity on electrical properties is very limited. Very likely, the non linear evolution of resistivity determined during the ERFS experiment (Fig. 5) can be related to the nature of the electrical contact points among WC nanoparticles. Two hypotheses can be advanced for such considerable resistivity reduction before sinter-

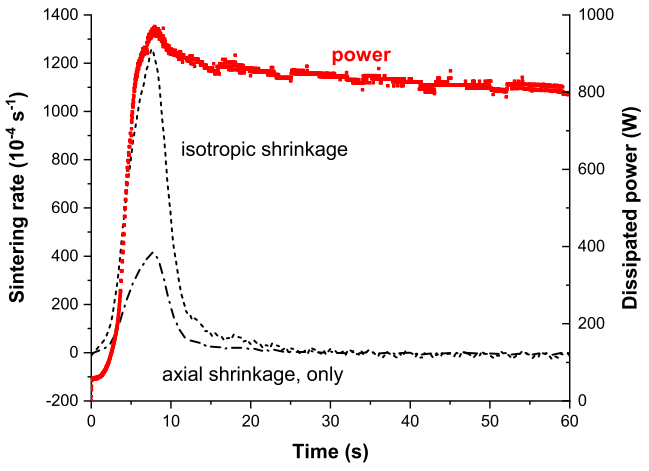

Fig. 7. Sintering rate during the process calculated from the vertical displacement recorded by the mechanical testing machine in the hypothesis of isotropic shrinkage and radial constraint; the power dissipated during the test is also shown.

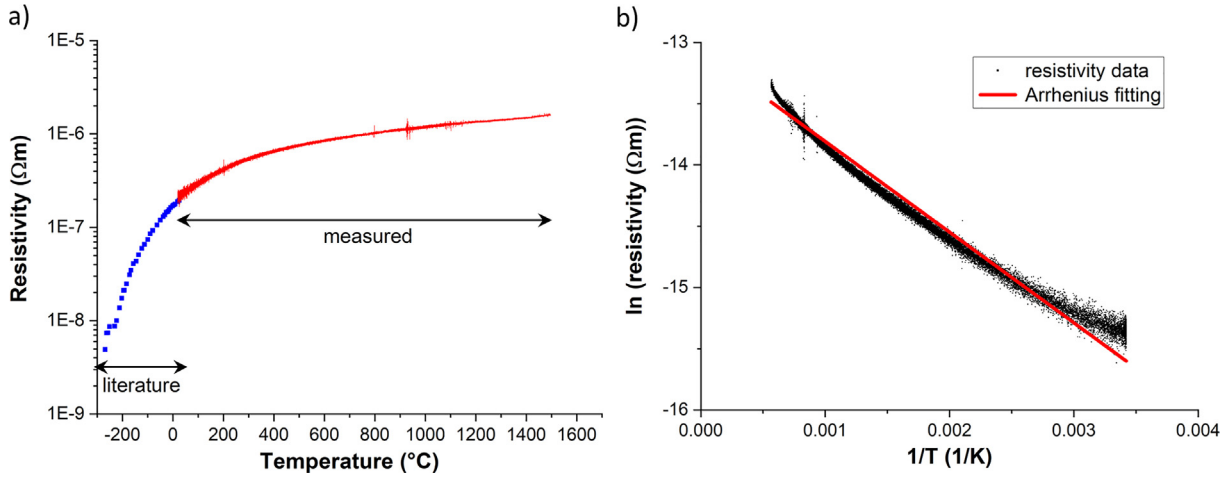

Fig. 8. Electrical resistivity of dense tungsten carbide (a): data in red are measured from 25 to 1500 °C on a sample produced by SPS while those in blue are taken from the literature [49]. The log form of the Arrhenius equation is shown in (b) by plotting log(resistivity) vs. 1/T.

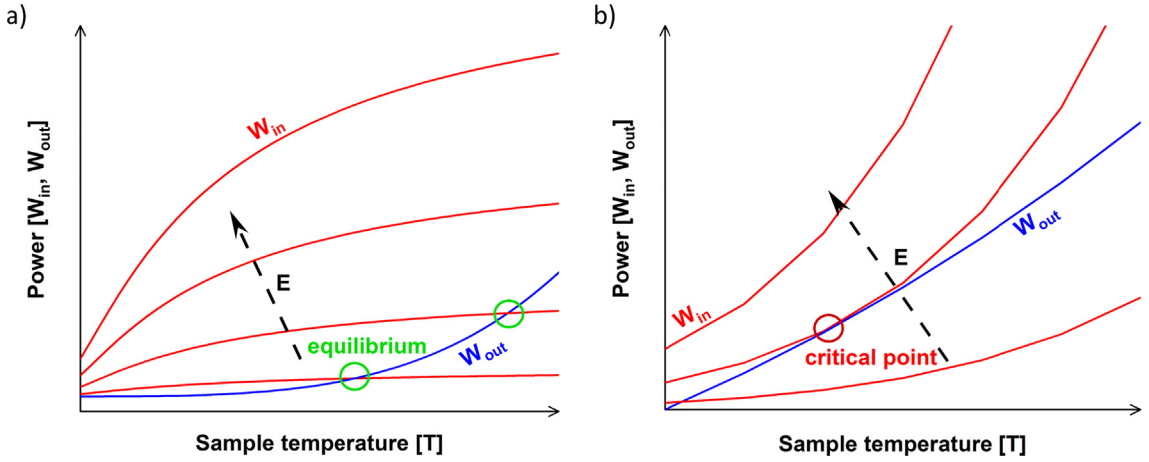

Fig. 9. Evolution of the heat generated by Joule heating (W_{in}) and of the heat dissipated by radiation (W_{out}) as a function of the sample temperature at increasing applied electrical field for (a) PTC and (b) NTC ceramic. W_{out} is evaluated in the former case considering only radiative losses and furnace temperature equals to room temperature.

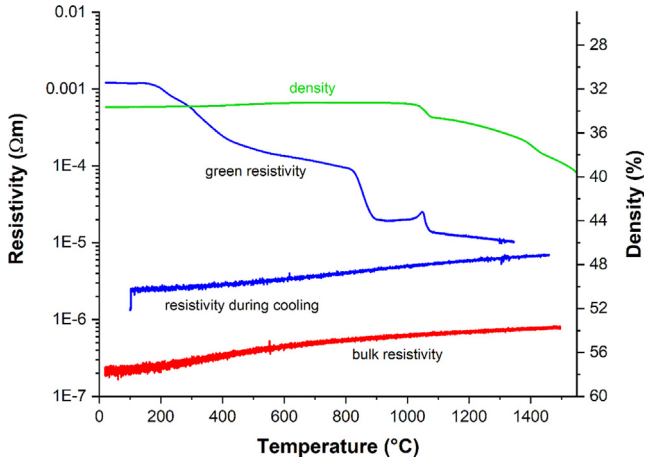

Fig. 10. Electrical resistivity and linear shrinkage (density curve) of a green WC pellet measured in a push rod dilatometer, increasing the temperature from 25 °C up to 1550 °C (10 °C/min) in Ar atmosphere. Resistivity was measure during both the heating and the cooling schedule.

ing: (1) the contact areas among particles increases due to surface diffusion phenomena (according to the constriction theory for small electrical contacts [51]) or (2) tungsten carbide surface chemistry changes with temperature because of the evolution of possible surface contaminants or oxides acting as resistive surface layers.

According to the first hypothesis, a larger applied pressure clearly affects the electrical contacts among particles and reduces the resistivity of the WC pellet in the zirconia die as shown in Fig. 11, the effect being independent on the pellet thickness (from 3.5 to 7.5 mm). The results in Fig. 11 confirm the very high initial green resistivity, with a difference between the green and bulk resistivity as high as four orders of magnitude at low pressure. A precise evaluation of the green resistivity is also crucial to determine a suitable contact pressure to minimize arc events and contacts overheating, thus homogenizing the current flow [52]. The initial resistivity of 40% dense green pellets is about $7.5x10^{-4}\Omega m$ at pressure of 4 MPa, as it was used in the experiment shown in Fig. 5. Such pressure minimizes the contact resistance with the Mo electrodes and helps to establish a good electrical contact during the ERFS process. The analysis of tungsten carbide surface chemistry and its possible role on the activation of the runaway

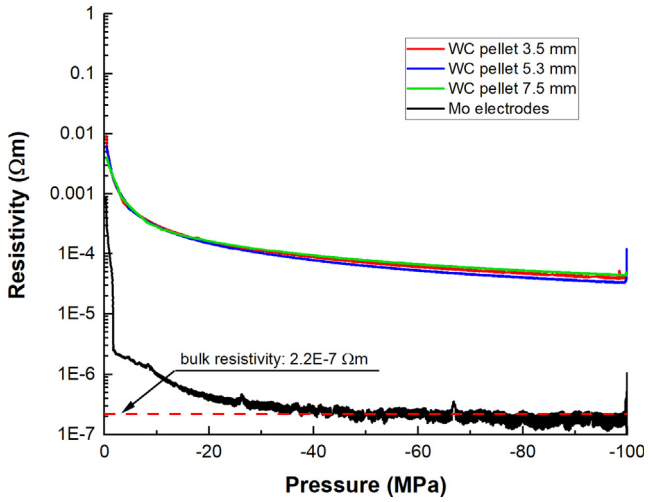

Fig. 11. Electrical resistivity of green WC pellets with different initial thickness and contact resistivity of the Mo electrodes. The resistivity of bulk WC is also indicated.

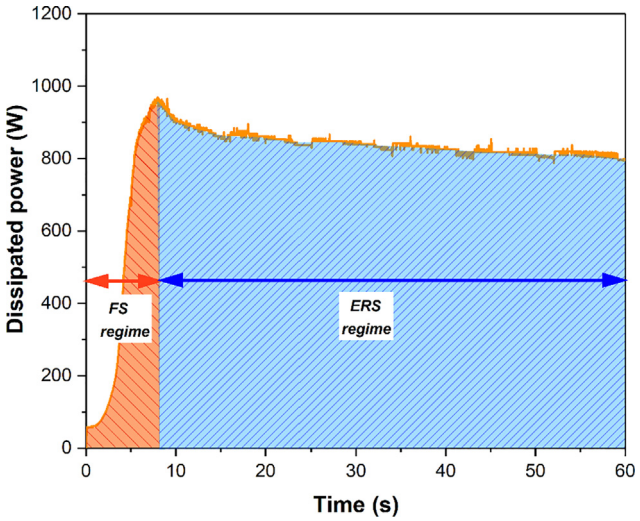

Fig. 12. FS and ERS regime as parts of the whole ERFS process.

event is beyond the aim of the present work and will be investigated in a forthcoming study.

The resistivity evolution during the first ERFS stages can explain the ultrafast densification of pure WC nanoparticles shown in Fig. 5. The initial NTC behaviour of the green pellet below 900 °C (Fig. 10) results in a very rapid resistivity reduction when an electrical current is applied (Fig. 5). Correspondingly, the superior resistivity of the sample shown in Fig. 11 accounts for the thermal runaway to occur for a certain transient period, thus determining an ultrafast temperature increase and sintering.

The data presented so far demonstrate that a "flash event" can therefore be triggered in metal like conductors in case of a transition in the conduction behaviour, from NTC to PTC. Unlike the flash behaviour of NTC ceramics, where the power supply limits the voltage or current, in the present case the process is controlled directly by the material nature and its structure. The power surge extinguishes by itself because of the different thermal runaway behaviour controlled by the high resistivity among particles and porosity. The avalanche phenomenon is continuous only for a particular combination of resistivity reduction and temperature increase. However, this iteration stops at a certain temperature, when the material passes from NTC to PTC behaviour, thus generating a self extinguishing feature.

3.3. How to achieve full densification

In order to analyse the phenomenology of the sintering process further, two regimes are identified during the entire sintering cycle as shown in Fig. 12 where the dissipated power plot previously described (Fig. 5) is reported. The initial one, whose duration is only a few seconds, is labelled as flash sintering (FS) regime, it being characterized by sudden evolution of resistivity, temperature and shrinkage. The second one, lasting for about a minute, is called electrical resistance sintering (ERS) regime, the material being Joule heated here under a constant current. The energy absorbed in the two regimes can be evaluated if one integrates the dissipated power in the time domain. The effect of the energy dissipated in the two regimes (FS and ERS) was analysed by changing the thickness of WC green pellets, applied voltage, pressure and time.

Fig. 13 shows how the thickness of the specimens influences both processing parameters (dissipated power, resistivity and temperature) and shrinkage upon the ERFS process. The fundamental parameters collected and calculated from the diagrams in Fig. 13 together with density and porosity measured on the sintered materials are reported in Table 1. The power peak is substantially constant, corresponding to a power density decreasing with the sample volumes, from 9700 down to 4400 mW/mm^3. Conversely, the density sensibly increases, from 57% to 73%, as the relative power peak diminishes. The recorded shrinkage and the microstructure analysed by SEM confirm an improvement in the densification as the sample thickness increases. As previously shown in Fig. 11, there is no difference in the resistivity of samples with various thicknesses which could justify the dissimilar densification. The only difference among the three flash events in Fig. 13 is the temporal occurrence of the power peak, which increases the resistivity and temperature evolution time scale. For 3.5 mm and 5.3 mm thick specimens, a maximum temperature around 1600 °C is reached at the power peak. For 7.5 mm sample, temperature increases over 1720 °C, as also proven by the thermocouple tip melting. This higher temperature advances the sintering to the II stage, with an evolution from the open porosity shown in Fig. 13(a, b) to the interconnected one of Fig. 13(c). This fact can be explained by comparing the energy consumed in the different sintering regimes. The total electrical energy is similar in the three cases (Table 1), this resulting in a lower specific energy available for thicker samples. Nevertheless, thicker samples reach larger density. The electrical energy fraction dissipated during the FS regime with respect to the total energy (Flash/total energy) increases with the duration of the power surge (FS regime duration in Fig. 12) as shown in Table 1: it appears clear that denser materials are obtained when a larger "Flash/total energy" is dissipated during the flash, this also corresponding to higher maximum temperature during the cycle. These observations also suggest a different efficiency of the energy dissipated during the power surge (Flash regime) with respect to that consumed upon the constant current regime (ERS regime). Therefore, the total energy is not the key factor for densification; conversely, it is the energy involved during flash regime which is somehow fundamental for the ERFS process.

The presence of a temperature peak as shown in Fig. 13 was also recorded in conventional flash sintering experiments [14,15,39,48,53]. Nevertheless, not in all scenarios the temperature peak arises in concomitance with the power peak. Ji et al. [26] found a maximum in temperature during the power surge before entering the constant current state, corresponding to the ERS regime in our case. Conversely, Raj et al. [39] modelled the flash temperature to occur just in the constant current regime, by accounting the energy generated during the power surge to be

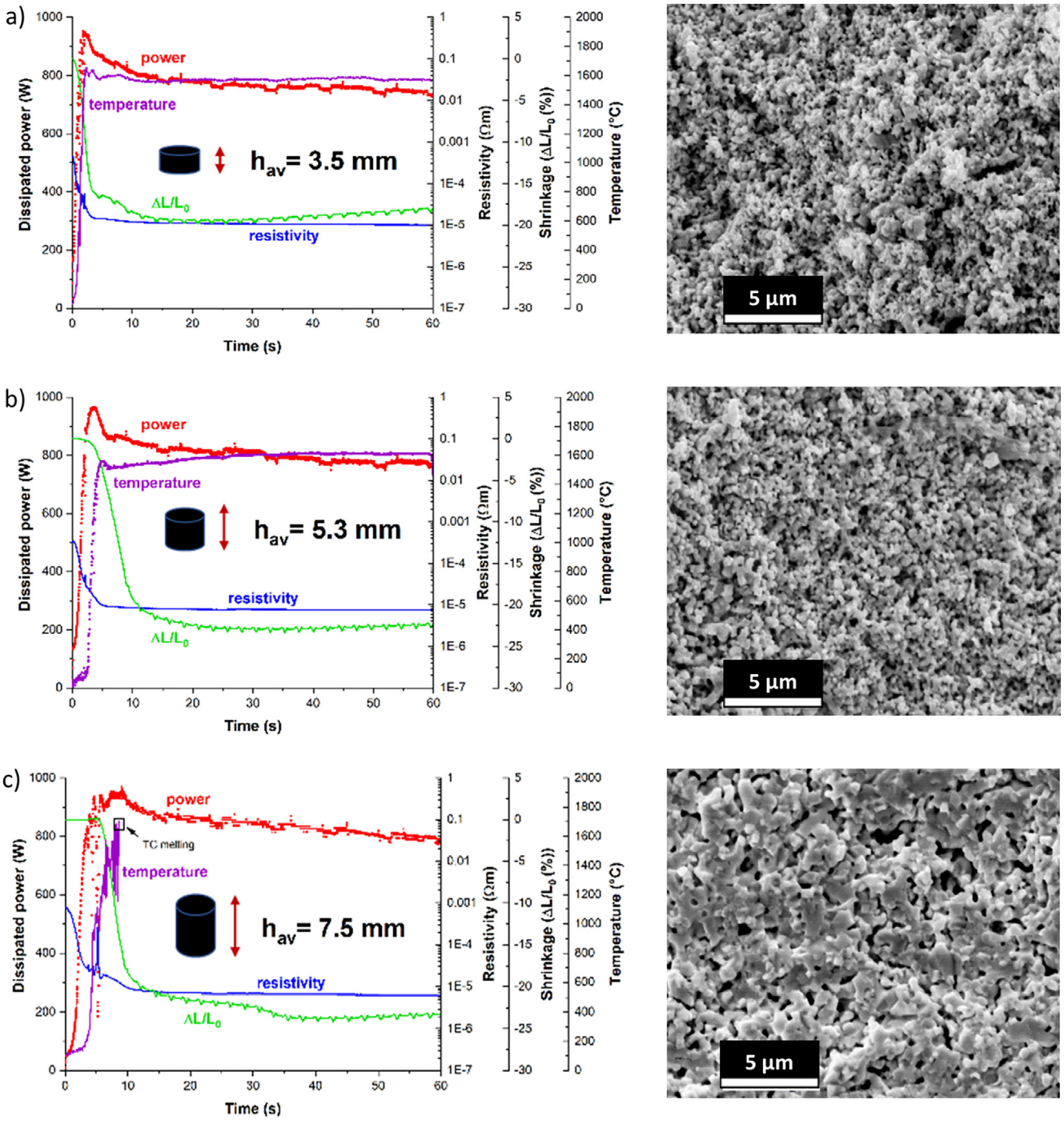

Fig. 13. Processing parameters and final microstructure of samples subjected to ERFS tests (3 V and 4 MPa) with initial thickness (h_{av}) equal to (a) 3.5 mm, (b) 5.3 mm and (c) 7.5 mm.

Table 1
Electrical parameters, relative density and apparent porosity for samples with different thickness subjected to ERFS.

Initial thickness	mm	3.5	5.3	7.5
Power peak	W	985 (±11)	963 (±5)	949 (±17)
Relative power peak	mW/mm^3	9748 (±250)	6477 (±181)	4448 (±460)
Current density‡	A/cm^2	3092 (±61)	2967 (±31)	2806 (±67)
Flash energy†	J/mm^3	12 (±1)	15.4 (±0.3)	24 (±4)
Total electric energy	J/mm^3	471 (±7)	326 (±1)	216 (±23)
	kJ	47.6 (±0.4)	48 (±1)	46 (±1)
Flash/total energy	%	3 (±1)	6 (±2)	13 (±4)
Density	%	57 (±6)	62 (±5)	73 (±3)
Apparent porosity	%	42 (±5)	33 (±6)	21 (±8)

(†) total energy provided to the material during the flash event (<10 s), calculated from the power integral up to the peak.
(‡) maximum current density recorded during the current control regime (>10 s).

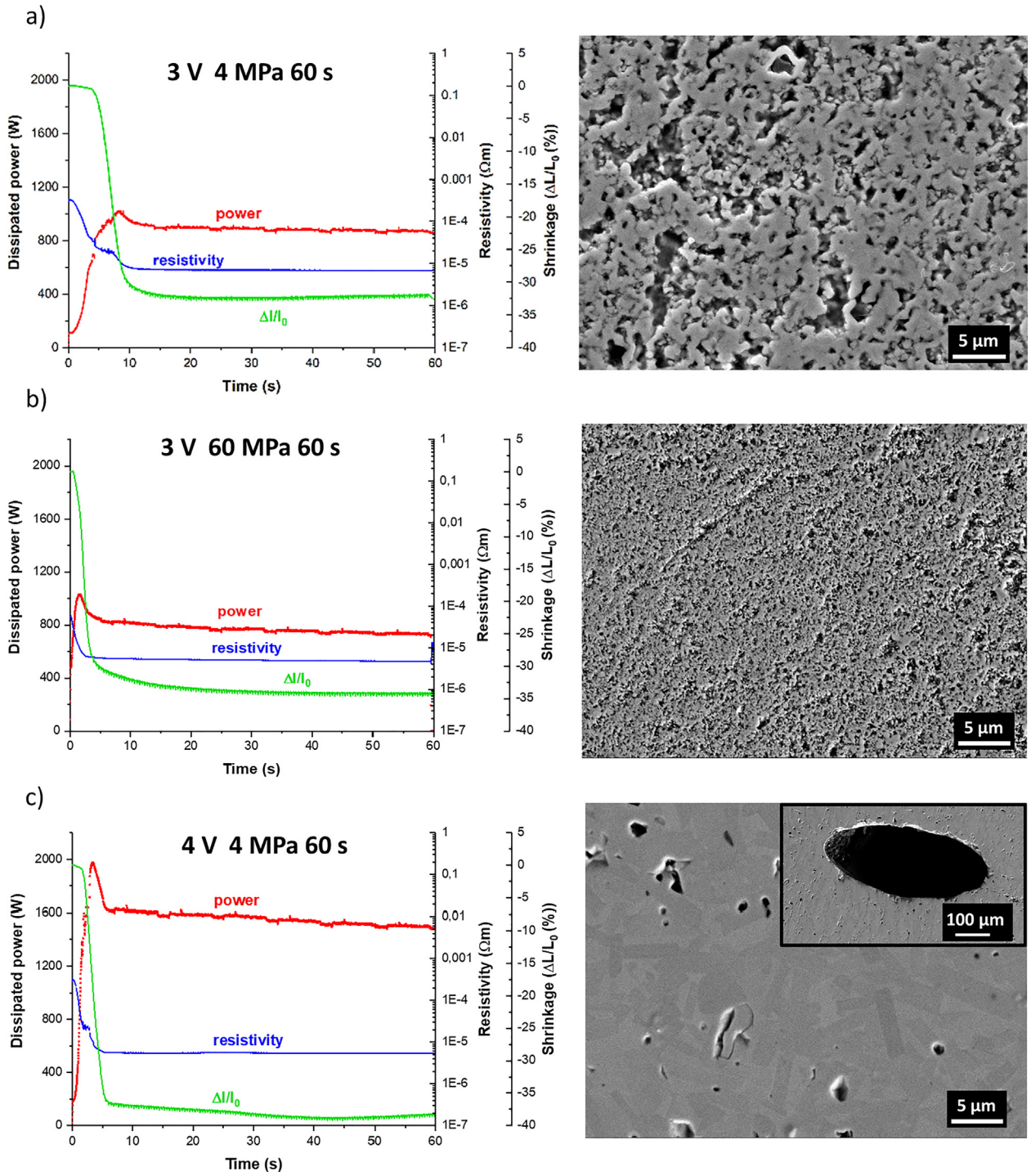

Fig. 14. Processing parameters and final microstructure of specimen subjected to 60 s-long ERFS tests by using different pressure and sintering voltage. An example of "hot spot" as formed in the central part of the pellet after sintering under 4 V is shown in the inset of (c)).

absorbed by the sample's heat capacity. Reasonably, for WC, the higher power achieved is no more comparable with its heat capacity (0.28 J/g K) and the heat generated during the power surge increases temperature to a maximum value before entering the steady state.

During the FS of NTC ceramics, the separation of field effects on matter transport phenomena from those related to the very fast heating rates is rather complicated. In the present work, the electric field is so weak that its effect, if any, is negligible. Ji et al. carried out an interesting work to separate the effects of electric field and heating rate, and they demonstrated an acceleration in the sintering rate by orders of magnitude for heating rates in the range $10^3 - 10^4$°C [26]. The higher efficiency of the electrical energy dissipated during the FS regime, where a thermal runaway occurs, can be connected to the exceptional heating and densification rates also measured in the present work. An extension of the flash period results in a higher sintering temperature and longer sintering time in the stage where the heating rate is accelerated. Zhang et al. [41] compared the effect of conventional and controlled FS experiments on zinc oxide, and they pointed out the importance of ultra high

Table 2
Electrical parameters, relative density and apparent porosity for samples sintered under different pressure and electric field.

		3 V 4 MPa 60 s	3 V 60 MPa 60 s	4 V 4 MPa 60 s	3.5 V 4 MPa 60 s	3.5 V 4 MPa 10 s
Power peak	W	949 (±17)	1032 (±8)	1977 (±12)	1585 (±25)	1519 (±20)
Relative power peak	W/mm^3	4448 (±460)	4675 (±15)	9504 (±150)	7259 (±70)	7260 (±50)
Current density‡	A/cm^2	2806 (±25)	3282 (±37)	4566 (±32)	3940 (±33)	3678 (±42)
Flash energy†	J/mm^3	24 (±4)	6 (±1)	19 (±1)	36 (±2)	30 (±2)
Total electric energy	J/mm^3	216 (±23)	209 (±14)	443 (±17)	369 (±11)	55 (±2)
Flash/total energy	%	13 (±4)	3 (±1)	4 (±1)	10 (±2)	55 (±3)
Density	%	73 (±3)	66 (±1)	96 (±1)	97 (±1)	95 (±2)
Apparent porosity	%	21 (±8)	31 (±2)	2 (±1)	1.5 (±0.5)	4.0 (±0.5)

(†) total energy provided to the material during the flash event (<10 s), calculated from the power integral up to the peak.
(‡) maximum current density recorded during the steady-state, current control regime (>10 s).

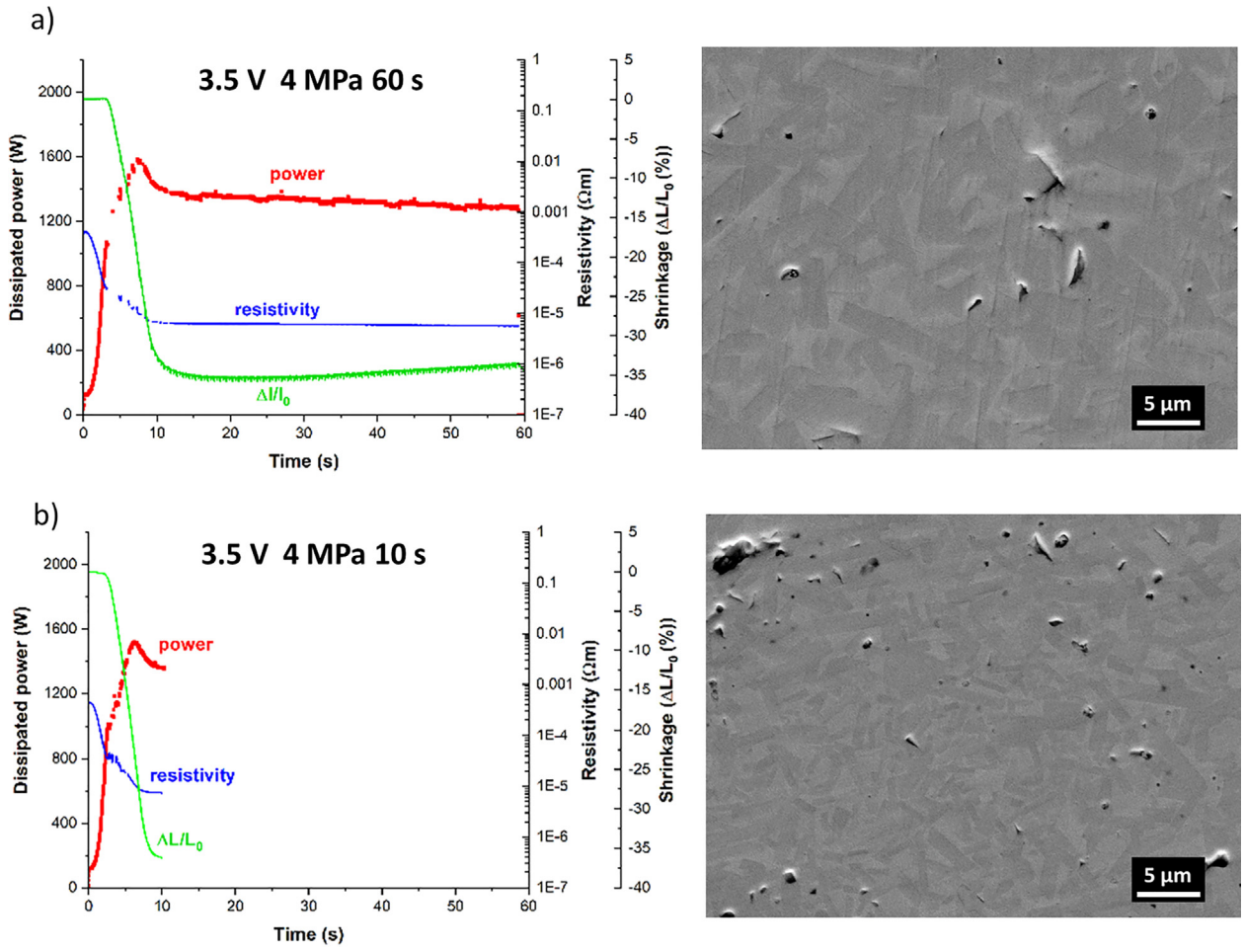

Fig. 15. Processing parameters and final microstructure of specimen subjected to ERFS tests at 3.5 V, 4 MPa after different sintering time of 60 s (a) and 10 s (b).

heating rates during the flash regime and the lower efficiency of the electrical energy dissipated in the steady current regime. Longer sintering times and more intense electrical energy generated by ramping up the current, step by step, did not increase the final density.

Fig. 14 shows the electrical parameters and shrinkage together with SEM micrographs taken on the cross section of materials sintered under different pressure and voltage. Quite surprisingly, the pellet subjected to high pressure is much less dense (Table 2). Nevertheless, such result can be explained based on previous arguments: (i) the initial green resistivity depends on the applied pressure (Fig. 11), which decreases abruptly down to $6x10^{-5}\Omega m$ at 60 MPa with respect to $7.5x10^{-4}\Omega m$ at 4 MPa; (ii) the onset time of the power peak is shortened, this resulting in much lower "Flash/total energy" ratio (Table 2). The higher pressure restricts the maximum evolution of resistivity by an order of magnitude and shortens the power surge duration, from 10 s to only 3 s as shown in Fig. 14. As reported in Table 2, the final density decreases from 73% to 66% when the pressure is increased from 4 to 60 MPa. The total electrical energy is the same and the only variable, which can justify the lower densification is the reduction in the "Flash/total energy" ratio from 13% to 3%.

A near full dense material is obtained by operating on the voltage (Fig. 14(c)). A higher voltage of 4 V doubles the available electric energy from 210 J/mm^3 (3 V) to around 450 J/mm^3 (Table 2), leading 96% dense material. However, due to such higher power,

excessive Joule heating causes hot spots in the central part of the sintered pellet, which limit the homogeneity of the final microstructure. It is interesting to point out that also the voltage affects the power surge duration (Fig. 14(a,c)) and, accordingly, the "Flash/total energy" ratio decreases from 13% (3 V) to just 4% (4 V).

Three variables are therefore found to affect the "Flash/total energy" ratio: i) pellet thickness, ii) applied pressure and ii) maximum voltage. Fig. 15 shows the microstructure of a 7.5 mm thick pellet sintered with an intermediate voltage of 3.5 V under 4 MPa pressure. Sintering with less intense voltage prevents the occurrence of hot spots, improves the homogeneity and allows to reach density as high 97%. To further prove the importance of the flash regime (FS) over the resistive heating one (ERS), the same experiment was carried out with duration of about 10 s, i.e., just after the flash event occurrence. The interruption of the current after the power peak increases the "Flash/total energy" ratio to 55% (Table 2), leading to a material with very high density (95%), limited porosity (4%) and homogeneous microstructure. This result confirms the different sintering behaviour in the FS regime with respect to the ERS one. The majority of the densification occurs during the power surge (Fig. 12) in the FS regime, during which the material behaves as a NTC ceramic and sintering occurs under a thermal runaway phenomenon. Densification slightly proceeds during the ERS regime where the material is characterized by a PTC behaviour and a more traditional resistive sintering takes place. These results agree with the previous hypothesis of higher efficiency of the electrical energy spent during the thermal runaway event, taking advantage of the ultra high heating rates, which boost the sintering rates by orders of magnitude. For comparison, sintering rate in the last case (Fig. 15) is about three times larger with respect to that estimated for the experiment in Fig. 5 ($900-3000x10^{-4}s^{-1}$ 3000x10vs. $400-1200x10^{-4}s^{-1}$). Such higher sintering rate coupled with a reduction of sintering time, from 60 to 10 s, is also much more energy efficient. If one compares the samples sintered under 3.5 V (60 s) and 3.5 V (10 s), the required energy enormously reduces from 369 J/mm^3 to just 55 J/mm^3 while the the density only decreased from 97% to 95% (Table 2).

The results achieved so far allow to propose a new processing route for the consolidation of tungsten carbide products, with important differences with respect the state of the art and, in particular, SPS process. It is worth to observe that the heating rate achievable during the flash regime in the ERFS process studied here is one two order of magnitude higher than in SPS process where it is usually around 50–1000 °C/min [36]. Accordingly, under the right flash conditions, the sintering rate is here at least ten times larger (0.2 s^{-1}) with respect to SPS (0.005 – 0.01 s^{-1}) [10]. The way in which the electric current interacts with the powder points out the differences between the two processes. In spite of some similarity, densification occurs here at a different time scale, leading to a great reduction in the time and the energy required for sintering. The possibility to tailor the final density and the microstructure of WC through the control of the ERFS operating conditions allows the production of materials specific for the particular application.

4. Conclusions

The application of high currents at moderate voltages to tungsten carbide green compacts is shown to induce nearly instantaneous densification of the material. The phenomenon responsible for such event is accounted for by a "flash event" where a thermal runaway phenomenon can be triggered thanks to the transition from NTC to PTC behaviour with temperature. Therefore, pure tungsten carbide can be densified up to 95% is less than 10 s. Pressure, electrical power, pellet thickness and sintering time have a prominent role in pure WC densification behaviour. Although the density does not reach 100% during the experiments carried out in the present work, the results demonstrate the possibility to sinter pure tungsten carbide in very short time and successive optimization procedures could guarantee to obtain fully dense materials. The possibility to obtain variable final microstructures by tuning the operating conditions appears challenging, as well. Finally, some differences can be pointed out here between the flash behaviour of NTC and PTC ceramics: i) the specific power peak values are here one two orders of magnitude larger, ii) the first stage of flash sintering is absent as no incubation time is necessary to initiate the current flow in a conductive powder and iii) the power surge event has a self extinguishing character.

CRediT authorship contribution statement

Isacco Mazo: Conceptualization, Methodology, Software, Validation, Formal analysis, Investigation, Data curation, Writing – original draft, Visualization, Project administration. **Alberto Molinari:** Resources, Writing – review & editing, Project administration. **Vincenzo M. Sglavo:** Writing – review & editing, Supervision, Resources, Funding acquisition, Project administration.

Declaration of Competing Interest

The authors declare that they have no known competing financial interests or personal relationships that could have appeared to influence the work reported in this paper.

Acknowledgements

We acknowledge Prof. Lucio Pancheri (University of Trento, Italy) for his assistance in the development of the data acquisition system and PhD Sofia Santi for the collaboration in the creation of the manuscript graphics.

Funding

This work is financially supported within the program Departments of Excellence 2018-2022 (DII-UNITN "E-Mat") – funded by the Italian Ministry of University and Research (MIUR).

Data availability

The raw/processed data required to reproduce these findings cannot be shared at this time as the data also forms part of an ongoing study.

Appendix A. Supplementary material

Supplementary data to this article can be found online at https://doi.org/10.1016/j.matdes.2021.110330.

References

[1] R.M. Raihanuzzaman, Z. Xie, S.J. Hong, R. Ghomashchi, Powder refinement, consolidation and mechanical properties of cemented carbides - An overview, Powder Technol. 261 (2014) 1–13, https://doi.org/10.1016/j.powtec.2014.04.024.
[2] J. García, V. Collado Ciprés, A. Blomqvist, B. Kaplan, Cemented carbide microstructures: a review, Int. J. Refract. Met. Hard Mater. 80 (2019) 40–68, https://doi.org/10.1016/j.ijrmhm.2018.12.004.
[3] X. Wu, J. Shen, F. Jiang, H. Wu, L. Li, Study on the oxidation of WC-Co cemented carbide under different conditions, Int. J. Refract. Met. Hard Mater. 94 (2021) 105381, https://doi.org/10.1016/j.ijrmhm.2020.105381.
[4] J. Sun, J. Zhao, Z. Huang, K.e. Yan, X. Shen, J. Xing, Y. Gao, Y. Jian, H. Yang, B.o. Li, A Review on Binderless Tungsten Carbide: Development and Application, A

Review on Binderless Tungsten Carbide: Development and Application 12 (1) (2020), https://doi.org/10.1007/s40820-019-0346-1.
[5] K. Kornaus, M. Rączka, A. Gubernat, D. Zientara, Pressureless sintering of binderless tungsten carbide, J. Eur. Ceram. Soc. 37 (15) (2017) 4567–4576, https://doi.org/10.1016/j.jeurceramsoc.2017.06.008.
[6] L. Silvestroni, N. Gilli, A. Migliori, D. Sciti, J. Watts, G.E. Hilmas, W.G. Fahrenholtz, Binderless WC with high strength and toughness up to 1500 °C, J. Eur. Ceram. Soc. 40 (6) (2020) 2287–2294, https://doi.org/10.1016/j.jeurceramsoc.2020.01.055.
[7] A. Nino, Y. Izu, T. Sekine, S. Sugiyama, H. Taimatsu, Effects of TaC and TiC addition on the microstructures and mechanical properties of Binderless WC, Int. J. Refract. Met. Hard Mater. 82 (2019) 167–173, https://doi.org/10.1016/j.ijrmhm.2019.04.012.
[8] S. Lay, A. Antoni-Zdziobek, J. Pötschke, M. Herrmann, Microstructural investigations in binderless tungsten carbide with grain growth inhibitors, Int. J. Refract. Met. Hard Mater. 93 (2020) 105340, https://doi.org/10.1016/j.ijrmhm.2020.105340.
[9] E.A. Lantsev, N.V. Malekhonova, V.N. Chuvil'deev, A.V. Nokhrin, M.S. Boldin, P. V. Andreev, K.E. Smetanina, Effect of initial particle size and various composition on the spark plasma sintering of binderless tungsten carbide, J. Phys. Conf. Ser. 1758 (1) (2021) 012022, https://doi.org/10.1088/1742-6596/1758/1/012022.
[10] E. Lantsev, N. Malekhonova, A. Nokhrin, V. Chuvil'deev, M. Boldin, Y. Blagoveshchenskiy, P. Andreev, K. Smetanina, N. Isaeva, S. Shotin, Influence of oxygen on densification kinetics of WC nanopowders during SPS, Ceram. Int. 47 (3) (2021) 4294–4309, https://doi.org/10.1016/j.ceramint.2020.09.272.
[11] E.A. Lantsev, N.V. Malekhonova, V.N. Chuvil'deev, A.V. Nokhrin, Y.V. Blagoveshchenskii, N.V. Isaeva, M.S. Boldin, P.V. Andreev, K.E. Smetanina, Binderless tungsten carbides with an increased oxygen content obtained by spark plasma sintering, J. Phys. Conf. Ser. 1758 (1) (2021) 012023, https://doi.org/10.1088/1742-6596/1758/1/012023.
[12] X. Liu, J. Zhang, C. Hou, H. Wang, X. Song, Z. Nie, Mechanisms of WC plastic deformation in cemented carbide, Mater. Des. 150 (2018) 154–164, https://doi.org/10.1016/j.matdes.2018.04.025.
[13] D. Garbiec, P. Siwak, Microstructural evolution and development of mechanical properties of spark plasma sintered WC–Co cemented carbides for machine parts and engineering tools, Arch. Civ. Mech. Eng. 19 (1) (2019) 215–223, https://doi.org/10.1016/j.acme.2018.10.004.
[14] M. Yu, S. Grasso, R. Mckinnon, T. Saunders, M.J. Reece, Review of flash sintering: materials, mechanisms and modelling, Adv. Appl. Ceram. 116 (1) (2017) 24–60, https://doi.org/10.1080/17436753.2016.1251051.
[15] M. Biesuz, V.M. Sglavo, Flash sintering of ceramics, J. Eur. Ceram. Soc. 39 (2-3) (2019) 115–143, https://doi.org/10.1016/j.jeurceramsoc.2018.08.048.
[16] M. Biesuz, S. Grasso, V.M. Sglavo, What's new in ceramics sintering? A short report on the latest trends and future prospects, Curr. Opin. Solid State Mater. Sci. 24 (5) (2020) 100868, https://doi.org/10.1016/j.cossms.2020.100868.
[17] M. Biesuz, V.M. Sglavo, Beyond flash sintering: How the flash event could change ceramics and glass processing, Scr. Mater. 187 (2020) 49–56, https://doi.org/10.1016/j.scriptamat.2020.05.065.
[18] X.L. Phuah, J. Cho, T. Tsakalakos, A.K. Mukherjee, H. Wang, X. Zhang, Defects in flash-sintered ceramics and their effects on mechanical properties, MRS Bull. 46 (1) (2021) 44–51, https://doi.org/10.1557/s43577-020-00014-y.
[19] R. Raj, A. Kulkarni, J.-M. Lebrun, S. Jha, Flash sintering: A new frontier in defect physics and materials science, MRS Bull. 46 (1) (2021) 36–43, https://doi.org/10.1557/s43577-020-00011-1.
[20] J. Li, J. Cho, J. Ding, H. Charalambous, S. Xue, H. Wang, X.L. Phuah, J. Jian, X. Wang, C. Ophus, T. Tsakalakos, R. Edwin García, A.K. Mukherjee, N. Bernstein, C. Stephen Hellberg, H. Wang, X. Zhang, Nanoscale stacking fault–assisted room temperature plasticity in flash-sintered TiO2, Sci. Adv. 5 (2019) 1–10, https://doi.org/10.1126/sciadv.aaw5519.
[21] J. Cho, Q. Li, H. Wang, Z. Fan, J. Li, S. Xue, K.S.N. Vikrant, H. Wang, T.B. Holland, A.K. Mukherjee, R.E. García, X. Zhang, High temperature deformability of ductile flash-sintered ceramics via in-situ compression, Nat. Commun. 9 (2018) 1–9, https://doi.org/10.1038/s41467-018-04333-2.
[22] A. Börger, J. Mertens, H. Wenzl, Thermal runaway and thermal runaway propagation in batteries: What do we talk about?, J Energy Storage. 24 (2019) 100649, https://doi.org/10.1016/j.est.2019.01.012.
[23] A. Eqbal, K.S. Arya, T. Chakrabarti, In-depth study of the evolving thermal runaway and thermal gradient in the dog bone sample during flash sintering using finite element analysis, Ceram. Int. 46 (8) (2020) 10370–10378, https://doi.org/10.1016/j.ceramint.2020.01.034.
[24] Y. Zhang, J. Il Jung, J. Luo, Thermal runaway, flash sintering and asymmetrical microstructural development of ZnO and ZnO-Bi2O3 under direct currents, Acta Mater. 94 (2015) 87–100, https://doi.org/10.1016/j.actamat.2015.04.018.
[25] E. Zapata-Solvas, D. Gómez-García, A. Domínguez-Rodríguez, R.I. Todd, Ultra-fast and energy-efficient sintering of ceramics by electric current concentration, Sci. Rep. 5 (2015) 1–7, https://doi.org/10.1038/srep08513.
[26] W. Ji, B. Parker, S. Falco, J.Y. Zhang, Z.Y. Fu, R.I. Todd, Ultra-fast firing: Effect of heating rate on sintering of 3YSZ, with and without an electric field, J. Eur. Ceram. Soc. 37 (6) (2017) 2547–2551, https://doi.org/10.1016/j.jeurceramsoc.2017.01.033.
[27] K. Ren, J. Liu, Y. Wang, Flash sintering of yttria-stabilized zirconia: Fundamental understanding and applications, Scr. Mater. 187 (2020) 371–378, https://doi.org/10.1016/j.scriptamat.2020.06.040.
[28] K.V. Kuskov, M. Abedi, D.O. Moskovskikh, I. Serhiienko, A.S. Mukasyan, Comparison of conventional and flash spark plasma sintering of cu–cr pseudo-alloys: Kinetics, structure, properties, Metals (Basel). 11 (2021) 1–16, https://doi.org/10.3390/met11010141.
[29] S. Grasso, T. Saunders, H. Porwal, O. Cedillos-Barraza, D.D. Jayaseelan, W.E. Lee, M.J. Reece, W. Fahrenholtz, Flash spark plasma sintering (FSPS) of pure ZrB2, J. Am. Ceram. Soc. 97 (8) (2014) 2405–2408.
[30] R. McKinnon, S. Grasso, A. Tudball, M.J. Reece, Flash spark plasma sintering of cold-Pressed TiB2-hBN, J. Eur. Ceram. Soc. 37 (8) (2017) 2787–2794, https://doi.org/10.1016/j.jeurceramsoc.2017.01.029.
[31] B. McWilliams, J. Yu, F. Kellogg, S. Kilczewski, Enhanced Sintering Kinetics in Aluminum Alloy Powder Consolidated Using DC Electric Fields, Metall. Mater. Trans. A Phys. Metall. Mater. Sci. 48 (2) (2017) 919–929, https://doi.org/10.1007/s11661-016-3861-4.
[32] B. McWilliams, J. Yu, F. Kellogg, Sintering aluminum alloy powder using direct current electric fields at room temperature in seconds, J. Mater. Sci. 53 (12) (2018) 9297–9304, https://doi.org/10.1007/s10853-018-2207-6.
[33] M. Jongmanns, R. Raj, D.E. Wolf, Generation of Frenkel defects above the Debye temperature by proliferation of phonons near the Brillouin zone edge, New J. Phys. 20 (9) (2018) 093013, https://doi.org/10.1088/1367-2630/aadd5a.
[34] Y. Liang, S. Xiang, T. Li, C. Yu, K.e. Leng, X. Zhang, Pressure-assisted flash sintering of ZnO ceramics, J. Am. Ceram. Soc. 104 (12) (2021) 6131–6143.
[35] C. Gorynski, U. Anselmi-Tamburini, M. Winterer, Controlling current flow in sintering: A facile method coupling flash with spark plasma sintering, Rev. Sci. Instrum. 91 (1) (2020) 015112, https://doi.org/10.1063/1.5119059.
[36] Z.-Y. Hu, Z.-H. Zhang, X.-W. Cheng, F.-C. Wang, Y.-F. Zhang, S.-L. Li, A review of multi-physical fields induced phenomena and effects in spark plasma sintering: Fundamentals and applications, Mater. Des. 191 (2020) 108662, https://doi.org/10.1016/j.matdes.2020.108662.
[37] M. Biesuz, J. Dong, S. Fu, Y. Liu, H. Zhang, D. Zhu, C. Hu, S. Grasso, Thermally-insulated flash sintering, Scr. Mater. 162 (2019) 99–102, https://doi.org/10.1016/j.scriptamat.2018.10.042.
[38] J.M. Montes, F.G. Cuevas, F. Ternero, R. Astacio, E.S. Caballero, J. Cintas, A method to determine the electrical resistance of a metallic powder mass under compression, Metals (Basel). 7 (2017) 1–9, https://doi.org/10.3390/met7110479.
[39] R. Raj, Joule heating during flash-sintering, J. Eur. Ceram. Soc. 32 (10) (2012) 2293–2301, https://doi.org/10.1016/j.jeurceramsoc.2012.02.030.
[40] E.A. Olevsky, S.M. Rolfing, A.L. Maximenko, Flash (Ultra-Rapid) Spark-Plasma Sintering of Silicon Carbide, Sci. Rep. 6 (2016) 1–9, https://doi.org/10.1038/srep33408.
[41] Y. Zhang, J. Nie, J.M. Chan, J. Luo, Probing the densification mechanisms during flash sintering of ZnO, Acta Mater. 125 (2017) 465–475, https://doi.org/10.1016/j.actamat.2016.12.015.
[42] S. Deng, R. Li, T. Yuan, P. Cao, S. Xie, Electromigration-Enhanced Densification Kinetics During Spark Plasma Sintering of Tungsten Powder, Metall. Mater. Trans. A Phys. Metall. Mater. Sci. 50 (6) (2019) 2886–2897, https://doi.org/10.1007/s11661-019-05201-4.
[43] C. Wang, W. Ping, Q. Bai, H. Cui, R. Hensleigh, R. Wang, A.H. Brozena, Z. Xu, J. Dai, Y. Pei, C. Zheng, G. Pastel, J. Gao, X. Wang, H. Wang, J.-C. Zhao, B. Yang, X.(. Zheng, J. Luo, Y. Mo, B. Dunn, L. Hu, A general method to synthesize and sinter bulk ceramics in seconds, Science 368 (6490) (2020) 521–526.
[44] R.F. Guo, H.R. Mao, Z.T. Zhao, P. Shen, Ultrafast high-temperature sintering of bulk oxides, Scr. Mater. 193 (2021) 103–107, https://doi.org/10.1016/j.scriptamat.2020.10.045.
[45] R.I. Todd, E. Zapata-Solvas, R.S. Bonilla, T. Sneddon, P.R. Wilshaw, Electrical characteristics of flash sintering: Thermal runaway of Joule heating, J. Eur. Ceram. Soc. 35 (6) (2015) 1865–1877, https://doi.org/10.1016/j.jeurceramsoc.2014.12.022.
[46] M. Yoshida, S. Falco, R.I. Todd, Measurement and modelling of electrical resistivity by four-terminal method during flash sintering of 3YSZ, J. Ceram. Soc. Japan. 126 (7) (2018) 579–590, https://doi.org/10.2109/jcersj2.17256.
[47] M.Z. Becker, N. Shomrat, Y. Tsur, Recent Advances in Mechanism Research and Methods for Electric-Field-Assisted Sintering of Ceramics, Adv. Mater. 30 (41) (2018) 1706369, https://doi.org/10.1002/adma.v30.4110.1002/adma.201706369.
[48] M. Cologna, B. Rashkova, R. Raj, Flash sintering of nanograin zirconia in <5 s at 850°C, J. Am. Ceram. Soc. 93 (2010) 3556–3559, https://doi.org/10.1111/j.1551-2916.2010.04089.x.
[49] W.S. Williams, Electrical properties of hard materials, Int. J. Refract. Met. Hard Mater. 17 (1-3) (1999) 21–26, https://doi.org/10.1016/S0263-4368(99)00005-0.
[50] M. Biesuz, P. Luchi, A. Quaranta, V.M. Sglavo, Theoretical and phenomenological analogies between flash sintering and dielectric breakdown in α-alumina, J. Appl. Phys. 120 (14) (2016) 145107, https://doi.org/10.1063/1.4964811.
[51] A. Mikrajuddin, F.G. Shi, H.K. Kim, K. Okuyama, Size-dependent electrical constriction resistance for contacts of arbitrary size: From Sharvin to Holm limits, Mater. Sci. Semicond. Process. 2 (4) (1999) 321–327, https://doi.org/10.1016/S1369-8001(99)00036-0.
[52] J.M. Montes, F.G. Cuevas, F. Ternero, R. Astacio, E.S. Caballero, J. Cintas, Medium-frequency electrical resistance sintering of oxidized C.P. iron powder, Metals (Basel) 8 (2018) 1–14, https://doi.org/10.3390/met8060426.
[53] E. Zapata-Solvas, S. Bonilla, P.R. Wilshaw, R.I. Todd, Preliminary investigation of flash sintering of SiC, J. Eur. Ceram. Soc. 33 (13-14) (2013) 2811–2816, https://doi.org/10.1016/j.jeurceramsoc.2013.04.023.